Talanta 288 (2025) 127709

Contents lists available at ScienceDirect

Talanta

journal homepage: www.elsevier.com/locate/talanta

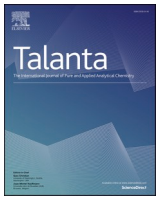

Integrating isothermal amplification techniques and LNA-based AI-assisted electrochemical bioassay for analysis of KRAS G12V point mutation

Ravery Sebuyoya [a], Sarka Sevcikova [a,b], Bolaji Yusuf [c], Martin Bartosik [a,*]

[a] Research Centre for Applied Molecular Oncology, Masaryk Memorial Cancer Institute, Zluty kopec 7, 656 53, Brno, Czech Republic
[b] National Centre for Biomolecular Research, Faculty of Science, Masaryk University, Kamenice 5, 625 00, Brno, Czech Republic
[c] Faculty of Information Technology, Brno University of Technology, Bozetechova 1/2, 612 00, Brno, Czech Republic

ARTICLE INFO

Handling Editor: Agata Michalska

Keywords:
Rolling circle amplification
Electrochemistry
Locked nucleic acid
KRAS gene
DNA point mutation

ABSTRACT

The *KRAS* mutation is a crucial biomarker for determining targeted cancer therapies, making its accurate and cost-effective detection vital for precision oncology. However, current methodologies, such as next-generation sequencing (NGS) or PCR-based methods, are often expensive and technically complex, limiting their accessibility. Here, we present a novel bioassay for *KRAS* G12V mutation analysis that combines rolling circle amplification (RCA) with locked nucleic acid (LNA)-modified magnetic beads, electrochemical detection using carbon electrode chips, and AI-assisted analysis via a logistic regression classifier. Our platform demonstrated exceptional selectivity in distinguishing the *KRAS* G12V mutation from wild-type (wt) sequences, enabling analysis <1 % of mutated DNA in a wt sample. We validated the bioassay on 7 cancer cell lines and 11 patient-derived samples, achieving results that perfectly correlated with NGS data. This innovative approach simplifies the workflow, reduces costs, and offers high sensitivity and specificity, making it a promising tool for clinical diagnostics and personalized cancer treatment strategies.

1. Introduction

Accurate identification of oncogenes is essential for monitoring cancer progression and selecting appropriate treatment. The *KRAS* gene is one of the most frequently mutated oncogenes in human cancers, particularly in colorectal (CRC), lung, and pancreatic tumors. Point mutations in *KRAS* play a crucial role in cancer progression by activating signaling pathways that promote cell proliferation and survival [1]. They are present in approx. 45 % of metastatic CRC tumors [2] and approximately 15 %–37 % of early stage tumors, making them resistant to EGFR therapy [3]. These mutations, especially at codons 12 and 13, are directly associated with the occurrence of poor prognosis and drug resistance and thus greatly impact therapeutic responses [4]. Among these mutations, G12V and G12D are the most common, accounting for about 60 % of pancreatic cancer, 20 % of colorectal cancer, and 8 % of non-small cell lung cancer [5,6]. Here, we focus on analysis of the *KRAS* G12V mutation (i.e., G35T substitution), which is present in ~8 % of CRC patients [7]. This mutation can serve as a predictive biomarker in targeted T-cell receptor (TCR) therapy since it produces a neoantigen presented by the HLA-A*11:01 molecule, allowing for the development of TCRs that can accurately recognize and target cancer cells with this mutation, hence improving the specificity and effectiveness of the immunotherapy [8]. The prevalence of these mutations underscores the urgency of the issue in cancer diagnosis and treatment.

While next-generation sequencing (NGS) of DNA from solid tumors remains the gold standard for diagnosing point mutations in the *KRAS* gene [9], it has several limitations in terms of high cost, complex data analysis, and time-consuming protocols. On the other hand, PCR-based methods, such as the amplification refractory mutation system (ARMS) or Real-Time PCR require thermal cyclers and are prone to PCR inhibitors that decrease efficiency of the reaction. Other techniques, such as restriction fragment length polymorphism requires specific restriction enzymes and denaturing high-performance liquid chromatography faces challenges in detecting heterozygous mutations [10]. These limitations highlight the urgent need for more efficient and cost-effective methods to detect DNA point mutations.

An interesting alternative to PCR are isothermal amplification techniques (IATs) that operate at ambient constant temperatures and can amplify both DNA or RNA at short times under 1 h. IATs, such as rolling circle amplification (RCA), loop-mediated amplification (LAMP),

This article is part of a special issue entitled: Electroanalysis published in Talanta.

* Corresponding author.
E-mail address: martin.bartosik@mou.cz (M. Bartosik).

https://doi.org/10.1016/j.talanta.2025.127709
Received 29 November 2024; Received in revised form 5 February 2025; Accepted 7 February 2025
Available online 7 February 2025
0039-9140/© 2025 The Authors. Published by Elsevier B.V. This is an open access article under the CC BY license (http://creativecommons.org/licenses/by/4.0/).

or recombinase polymerase amplification (RPA), have become popular due to their speed, easy operation, simple instrumentation and high sensitivity [11–15]. Among these, RCA is well-suitable for detecting point mutations. During the RCA reaction, the target DNA or RNA hybridizes with the specially designed padlock probe (PP) modified with a phosphate group at its 5' end. This phosphate modification facilitates the ligation of the two terminal segments of the PP by covalently joining both ends with the ligase enzyme, yielding a circular template for the subsequent RCA reaction in the presence of phi29 polymerase, dNTPs and a primer. The RCA has been used and reported in various EC assays [16–18].

RCA, similarly as other IATs, is often coupled with electrochemical (EC) end-point detection to provide simple, rapid and cost-effective bioassays with low sample consumption, easy miniaturization or option of parallel measurements. While most assays show high sensitivity, they often lack clinical sample application (reviewed e.g. in Ref. [19]). Only minority of EC-based papers show application of the bioassay into the real clinical samples [20,21], including our recent EC work for analysis of *BRAF* V600E mutation that was applied to DNA samples from tumor tissues of melanoma and CRC patients [22]. Here, we present a bioassay that selectively discriminates wt and G12V mutation in the *KRAS* gene by using RCA reaction and locked-nucleic acid (LNA) probes that capture either wt or G12V RCA products, coupled to a rapid EC readout. Final bioassay was applied to a panel of 7 cancer cell lines and 11 CRC patient samples, showing very good concordance with sequencing data. Finally, we present a machine learning model to alleviate the human effort of interpreting the readouts. Specifically, we trained a logistic regression classifier which takes the readout and returns a binary decision on the presence or absence of the G12V mutation. Overall, our bioassay could be an interesting alternative for quick analysis of *KRAS* mutation important in CRC therapy management by offering rapid analysis time, low instrumentation costs and simplicity.

2. Material and methods

2.1. Material and apparatus

T4 DNA ligase, phi29 DNA polymerase, Fast Digest MspI enzyme, casein blocking buffer (CBB, marketed as Blocker™ Casein), and streptavidin-peroxidase polymer (SPP, sold as poly-HRP streptavidin) were obtained from Thermo Fisher Scientific (USA). Biotin-16-dUTP (biotin-dUTP) was purchased from Jena Bioscience (Germany), and the dNTP mix came from Serva (Germany). Sera-Mag™ SpeedBead carboxylate-modified magnetic particles (MPs) were obtained from Cytiva (USA). Hydroquinone (HQ) was acquired from Sigma-Aldrich (USA), and the TwistAmp® Basic Kit for RPA reactions was provided by TwistDx Limited (UK). The Carl Roth GmbH (Germany) supplied agarose for gel electrophoresis, and GelRed nucleic acid gel stain was obtained from Biotium (USA). Gel electrophoresis was run using sub-cell GT and Mini-sub-cell GT cells (Bio-Rad, USA). DNA oligonucleotides (including synthetic targets, primers, and PPs) were synthesized by Generi Biotech (Czech Republic) while LNA-containing capture probes (CPs; marketed as Affinity Plus single-stranded DNA) were obtained from Integrated DNA Technologies (USA). Their sequences are detailed in Table 1.

The multipotentiostat/galvanostat μStat 8000 (Metrohm DropSens, Spain) was connected to an EC array of eight cells, each configured in a three-electrode setup (Metrohm DropSens, DRP-8X110) and controlled by DropView software. The three-electrode configuration included carbon working, auxiliary electrodes, and a pseudo-reference silver electrode. A suitably sized magnetic support was placed beneath the array.

2.2. Cell lines and clinical samples

Human colorectal adenocarcinoma cell lines HT-29, SW-480 and SW-620, lung carcinoma cell line A549, cervical carcinoma cell line HeLa and malignant melanoma cell line A375 were maintained in Dulbecco's modified Eagle's medium. Colorectal adenocarcinoma cell line DLD-1 and cervical carcinoma cell line CaSki were maintained in RPMI 1640 medium. All cell lines were supplemented with 1 % pyruvate, penicillin-streptomycin (Biosera, France), and 10 % FBS (Fetal Bovine Serum from Gibco, USA), and grown at 37 °C under a humidified atmosphere of 5 % CO_2. We used the Tissue DNA Preparation Column Kit (Jena Bioscience, Germany) following the manufacturer's instructions for DNA extraction.

The study was approved by the Ethical Committee of Masaryk Memorial Cancer Institute (2020/1471/MOU), and informed consent was obtained from all patients enrolled in the study. DNA extraction from formalin-fixed paraffin-embedded tissues was performed using the QIAamp DNA FFPE Tissue Kit (Qiagen, Germany), following the manufacturer's instructions. DNA concentration was measured using a Qubit Fluorometer 3.0 with the Qubit® dsDNA HS Assay Kit (Thermo Fisher Scientific, USA). Sequencing was conducted on a MiSeq instrument (Illumina, USA), and mutation status evaluation was performed using NextGENe software (SoftGenetics, USA). The minimum allele frequency was set to 5 %, and the minimum coverage of sequenced regions (300 ×) was verified using IGV (Broad Institute) and NextGENe.

2.3. RPA pre-amplification protocol

The RPA reaction was used to pre-amplify genomic DNA from cancer cells and patient samples to obtain shorter DNA fragments. Following the manufacturer's recommendations, we employed the TwistAmp® Basic Kit (TwistDx Ltd, UK) with a supplied 96-well plate. Briefly, lyophilized reagents in a well were reconstituted (in this order) with 29.5 μL of rehydration buffer, 2.4 μL of 10 μM forward RPA primer, 2.4 μL of 10 μM reverse RPA primer, 100 ng of cell DNA, and 2.5 μL of 280 mM magnesium acetate to initiate the reaction. The mixture was incubated in a thermoblock for 20 min at 39 °C, visualized with gel electrophoresis, and subsequently used as a template DNA in the RCA

Table 1
List of oligonucleotide sequences used in the study. Underlined letter indicates mutation (i.e. position of G35T substitution in codon 12, GGT→GTT). Bold letters indicate codon 12 triplet. Plus sign (+) denotes LNA base.

Oligonucleotide	Sequence 5′- 3′
RCA primer	TCAGCACTAACGTCAACGCGTGCTGAAGTCAAGTT
wt padlock probe (wt PP)	5′-phosphate-CAGCTCCAACTACAGAGCGCATGAATCCGTAGTAACTTGACTTCAGCACGCGTGAGGCCGGTACATCTCCTCTTGCCTACGCCA**C**
G12V padlock probe (G12V PP)	5′-phosphate-CAGCTCCAACTACAGAGCGCATGAATCCGTAGTAACTTGACTTCAGCACGCGTGAGGCCGGTACATCTCCTCTTGCCTACGCCA**A**
wt target	CTAATATAGTCACATTTTCATTATTTTTATTATAAGGCCTGCTGAAAATGACTGAATATAAACTTGTGGTAGTTGGAGCT**GGT**GGCGTAGGCAAGAG
wt complement	CTCTTGCCTACGCC**ACC**AGCTCCAACTACCACAAGTTTATATTCAGTCATTTTCAGCAGGCCTTATAATAAAAATAATGAAAATGTGACTATATTAG
G12V target	CTAATATAGTCACATTTTCATTATTTTTATTATAAGGCCTGCTGAAAATGACTGAATATAAACTTGTGGTAGTTGGAGCT**G<u>T</u>T**GGCGTAGGCAAGAG
G12V complement	CTCTTGCCTACGCC**AA<u>C</u>**AGCTCCAACTACCACAAGTTTATATTCAGTCATTTTCAGCAGGCCTTATAATAAAAATAATGAAAATGTGACTATATTAG
wt LNA CP	CCTAC+**G**+**C**+CACCAGCT-NH_2
G12V LNA CP	TACGCC+**A**+**A**+**C**AGCTCC-NH_2
RPA forward primer	GGTGAGTTTGTATTAAAAGGTACTGG
RPA reverse primer	TTAGCTGTATCGTCAAGGCACTC

reaction (see section "Rolling Circle Amplification").

2.4. Rolling circle amplification

The RCA reaction was performed as reported in our previous work [22] with slight modifications. The target DNA (i.e., synthetic *KRAS* target duplex DNA having either wt or G12V sequence, see Table 1, or DNA from cell lines/patients tissue) was mixed with 100 nM of the corresponding PP (wt PP or G12V PP) and 100 nM RCA primer in PBS. This DNA mixture was initially denatured at 95 °C for 5 min and rapidly cooled on ice. A ligation step followed to seal the gap between the 5′ and 3′ ends of the PP when it hybridized with the target sequence. The ligation reaction comprised the denatured DNA mixture, 2 units of T4 ligase, 0.2 M NaCl and 1 × ligation buffer (supplied as a 10 × stock) and the reaction was incubated at 30 °C for 30 min, with enzyme inactivation at 65 °C for 10 min.

Following ligation, the RCA reaction was initiated by mixing 10 μL of the ligation product with 1 × RCA buffer, 0.4 mg/mL BSA, 0.2 mM dNTPs, 12.5 μM biotin-dUTP, and 3 U of phi29 polymerase in a final volume of 40 μL. The reaction was incubated at 30 °C for 60 min. The amplified RCA products were subsequently digested using MspI enzyme in 1 × Fast Digest buffer at 37 °C for 30 min and visualized via gel electrophoresis (1.5 % agarose gel stained with GelRed). The RCA product were then added to LNA-modified MPs, as detailed in the subsequent procedure.

2.5. Modification of magnetic particles with LNA probes

Carboxylated MPs were coupled with amino-modified LNA probes in following way. Twenty μL of MPs were washed three times with 190 μL 25 mM MES buffer (pH 5.0), and resuspended in the same 25 mM MES buffer. Then, 20 μL of 100 μM LNA CPs (2 nmol) were added to MPs and incubated for 30 min at room temperature (RT) without a washing step, followed by an addition of 30 μL of 100 mg/mL EDC dissolved in MES buffer for 2 h at 4 °C. The LNA-modified MPs were washed three times with 190 μL of PBS, and supplemented with 200 μL of 0.02 % sodium azide (in PBS) to improve stability. Final mixture was stored at 4 °C for future use.

2.6. Hybridization at magnetic particles

After the RCA reaction, 1 μL of LNA-modified MPs were washed three times with 100 μL washing buffer (1 M NaCl, 0.5 mM EDTA, 5 mM Tris-HCl, pH 7.5) and incubated with 3 μL RCA-digested product in 0.3 M NaCl at 37 °C for 30 min. The mixture was then washed three times with CBB and incubated with 25 μL SPP (diluted 1:2000 in CBB) for 30 min at RT. Finally, the MPs were washed three times with 0.1 M phosphate buffer (PB; pH 6.0) and resuspended in 15 μL of the same buffer for amperometric measurements.

2.7. Electrochemical readout

Resuspended MPs were dropped onto the working electrode surface of the screen-printed EC chip with the magnetic support under the chip to pre-concentrate MPs on the surface. MPs were then covered with 50 μL substrate solution containing 10 mM hydroquinone and 50 mM H_2O_2 in PB. Electrical current from the reduction of enzymatically oxidized hydroquinone was measured amperometrically at −0.3 V for 90 s.

2.8. Statistical analysis

The Mann–Whitney nonparametric unpaired test was applied to determine whether there is a significant difference between the wt and mutated samples. Data for *p*-values were calculated from the mean values of EC signals. The *p*-value below 0.05 was considered significant.

2.9. Logistic regression classifier

A logistic regression model was used to automate the decision-making process. Given the sequence of currents, the model was trained to return a probability that the G12V mutation has occurred, i.e., it returns a single number between 0 and 1, with 0 indicating high certainty that no mutation was detected, and 1 indicating high certainty that the mutation was detected. For each sample, the input to the classifier was a vector constructed by concatenating the current values from the two padlocks. Instead of the current values directly, their logarithms were used as the classifiers input features, effectively amplifying differences in low-amplitude regions of the signal. Furthermore, 1 was added to each value to avoid potentially taking logarithms of 0. Thus for each current value, x, the input feature was log(1+x). This resulted in a 362-dimensional feature vector since each readout comprised 181 current values (one every 0.5 s for 90 s), and thus the logistic regression model had 362 trainable weights and a trainable bias term. Samples were split into train and test sets with the former used to learn the weights of the model which was then evaluated on the latter. Given the low number of samples, the model was evaluated using a leave-pair-out cross-validation scheme, i.e., three samples were held out as test set while the model was trained on the remaining samples; then the aggregate performance of the model over all such combinations was reported.

As pre-processing, each feature dimension was z-score normalized, i.e., the per-dimension mean values and standard deviations of the features were computed from the training set for the respective cross-validation fold. Then the mean was subtracted from the feature and the result was divided by the standard deviation to yield the final input representation. The model was built using the Scikit-learn Python library [23]. L1-regularization was applied with inverse regularization strength set to C = 5 to encourage sparse feature utilization.

3. Results and discussion

3.1. Principles of the bioassay

The proposed bioassay consists of multiple stages, as outlined in the workflow (Fig. 1). When clinical samples are involved, the initial stage first involves tumor tissue biopsy (Fig. 1, step 1), followed by DNA extraction step (Fig. 1, step 2). In case of cancer cell lines, the first step is omitted, starting with the DNA extraction. Then, the genomic DNA is pre-amplified using RPA reaction that generates small DNA fragments of defined length (similar to PCR amplicons) (Fig. 1, step 3). These fragments then serve as a target DNA for RCA reaction that follows in the next step. All these preceding steps can be omitted when working with synthetic model DNA (Table 1), but they are required once the cell lines or clinical samples are used.

Recognition of the DNA mutation itself takes place in the next steps. For this purpose, one universal primer and two different PPs for *KRAS* gene were designed, one targeting wt DNA and the other one targeting DNA carrying the G35T mutation (i.e., G12V mutation). The wt PP had a cytosine at its 3′-end to complement the guanine at that particular position in the codon 12 (underlined G in the GGT triplet of the target), while the G12V PP featured an adenine at its 3′-end to pair with the thymine in codon 12 (underlined T in the GTT triplet in the target) (Fig. 1, step 4 and Table 1).

Next stage involved DNA ligation of 5′ and 3′-ends of a PP molecule (Fig. 1, step 5), which was designed in such a way that both terminal regions were complementary to adjacent sections of the target DNA sequence, bringing these ends together upon hybridization. The ends of the PP molecule were covalently linked by the T4 ligase enzyme only when the 3′-end of the PP perfectly matched the target sequence. In other words, ligation occurred only when wt target bound with wt PP, or when G12V target bound with G12V PP, but not in other combinations. The result of this ligation was a covalently closed circular PP, which then

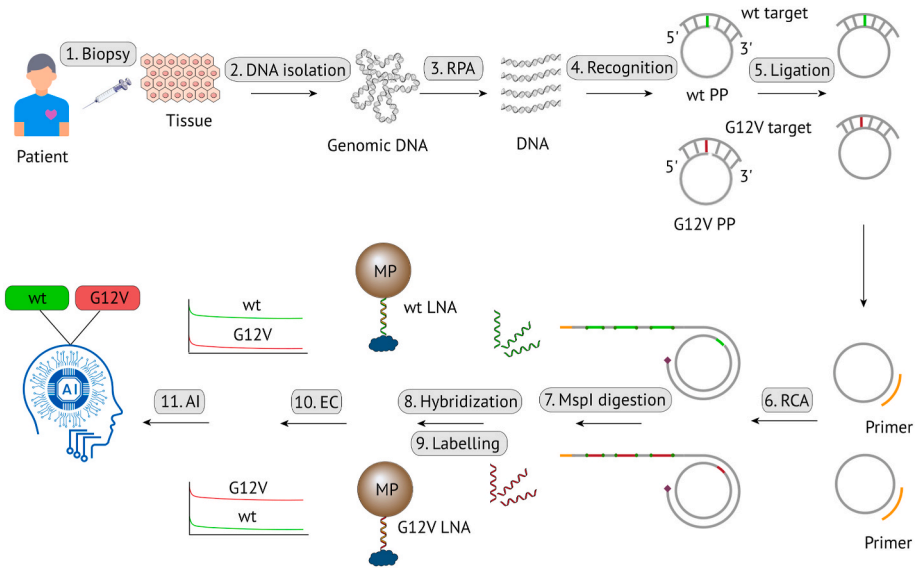

Fig. 1. The scheme of the bioassay workflow, divided into B_{WT} path (with green target) and B_{G12V} (with red target), comprising 1) collection of patient samples, 2) DNA isolation, 3) RPA pre-amplification to obtain shorter DNA fragments, 4) binding of RPA fragments to corresponding padlock probes (wt PP/G12V PP), 5) ligation of PP ends to create circular template, 6) amplification of the template with RCA reaction, 7) enzymatic digestion, 8) hybridization of the RCA digested products at LNA-modified magnetic particles and 9) subsequent binding of SPP (blue), 10) EC readout and 11) final AI-assisted decision using logistic regression analysis. RPA - recombinase polymerase amplification; MP – magnetic particle; LNA - locked nucleic acid.

acted as the template for the subsequent RCA reaction (Fig. 1, step 6). During the RCA, phi29 polymerase elongated the primer's 3′-end along the PP circle to generate huge RCA product composed of many repeating PP sequences. Moreover, phi29 polymerase is capable of inserting modified nucleotides into the growing strand [22,24]; thus we added into our reaction, besides classical unmodified mixture of four dNTPs, also biotinylated dUTPs that were randomly incorporated instead of dTTP. Afterwards, to facilitate binding of the huge RCA product to MPs (see below), an enzymatic fragmentation step was included (Fig. 1, step 7). The RCA product was digested using the restriction endonuclease MspI that specifically cleaves dsDNA at the CCGG restriction site, which was intentionally incorporated into both wt PP and G12V PP during their design.

Such fragmented RCA products were then captured using complementary LNA probes in a highly selective manner (Fig. 1, step 8). LNA probes contained amino modifier at their 3′-end to be attached to carboxylated MPs via EDC chemistry. Two types of LNAs were used, one complementary to wt sequence of the *KRAS* gene, the other to the G12V sequence. For a sake of clarity, the part of the bioassay involving wt PP and wtLNA will be referred to as wt biosensor (B_{WT}), and the part involving G12V PP and G12V LNA will be G12V biosensor (B_{G12V}). After successful hybridization of RCA products to LNA-modified MPs, a streptavidin-peroxidase polymeric conjugate was introduced to bind with biotin moieties incorporated during the RCA reaction (Fig. 1, step 9), an enzymatic reaction was monitored with amperometry (Fig. 1, step 10) and automatically classified with logistic regression analysis (Fig. 1, step 11). Despite involving several steps, the bioassay is simple and relatively fast, completed in approx. 3 h.

The assay operates in a dual-mode by dividing each sample into two separate tubes: one containing the wt PP and the other containing the G12V PP. Both tubes are processed in parallel, ultimately resulting in two distinct outputs per sample - one current value for the B_{WT} and another for the B_{G12V}. This approach offers a significant advantage by reducing the likelihood of false negatives. Specifically, a sample is expected to yield a positive result for at least one of the padlocks (either wt PP or G12V PP). If both outputs are negative, it indicates that the assay did not perform as intended and requires repetition.

3.2. Optimization steps

In this assay, we optimized various parameters, including the volume of MPs, NaCl concentration, SPP dilution, and hybridization temperature. MP volumes ranging from 1 μL to 5 μL were tested, revealing that lower MP volumes actually increased the signal-to-noise ratio (S/N) (Fig. 2A). Working with <1 μL volumes becomes challenging due to possible pipetting errors and mainly due to a fact that such low volumes become hardly visible during the washing. Consequently, 1 μL of MPs was chosen, yielding a wt-to-G12V ratio of 4.22 when using wt PP. This signal-to-noise ratio was still relatively low and may have been influenced by the low efficiency of ligase, which can be improved with supplements such as NaCl, PEG, ATP, $MgCl_2$, and DTT [25]. Indeed, when we investigated an effect of NaCl addition, the ratio significantly increased with this NaCl supplement (almost 10-times higher S/N when using NaCl, Fig. 2B).

We also optimized the SPP dilution, testing various concentrations and found that a 1/2000 dilution provided an optimal S/N (Fig. 2C). Finally, we evaluated the hybridization temperature for the LNA CP and RCA digested amplicons. Although high wt-to-G12V ratios were consistent across temperatures (Fig. 2D), we selected 37 °C to match the assay's overall temperature conditions (this temperature also provided the highest S/N). Additional parameters were optimized based on our previous publications [22,26–30].

3.3. Analytical characteristics

After optimizing the key assay parameters, we constructed a calibration curve to evaluate the B_{wt} detection limit using wt target DNA with wt PP and wt LNA-MPs (Fig. 3A). Target DNA concentrations ranged from 0 to 500 nM (including 0.1, 0.5, 1, 2, 3, 4, 5, 10, 100, and 500 nM). A linear detection range was observed between 0.5 nM and 10 nM, with an R^2 value of 0.9905 and a slope of 5.502 ± 0.219 μA nM^{-1} (Fig. 3B). The limit of detection (LOD) was calculated as 61 pM, based on three times the standard deviation of ten blank measurements divided by the slope. The limit of quantification (LOQ) was calculated as 205 pM, using ten times the standard deviation divided by the slope. Measurements were performed in duplicates. To assess assay reproducibility, we conducted eight parallel measurements with 5 nM wt DNA target,

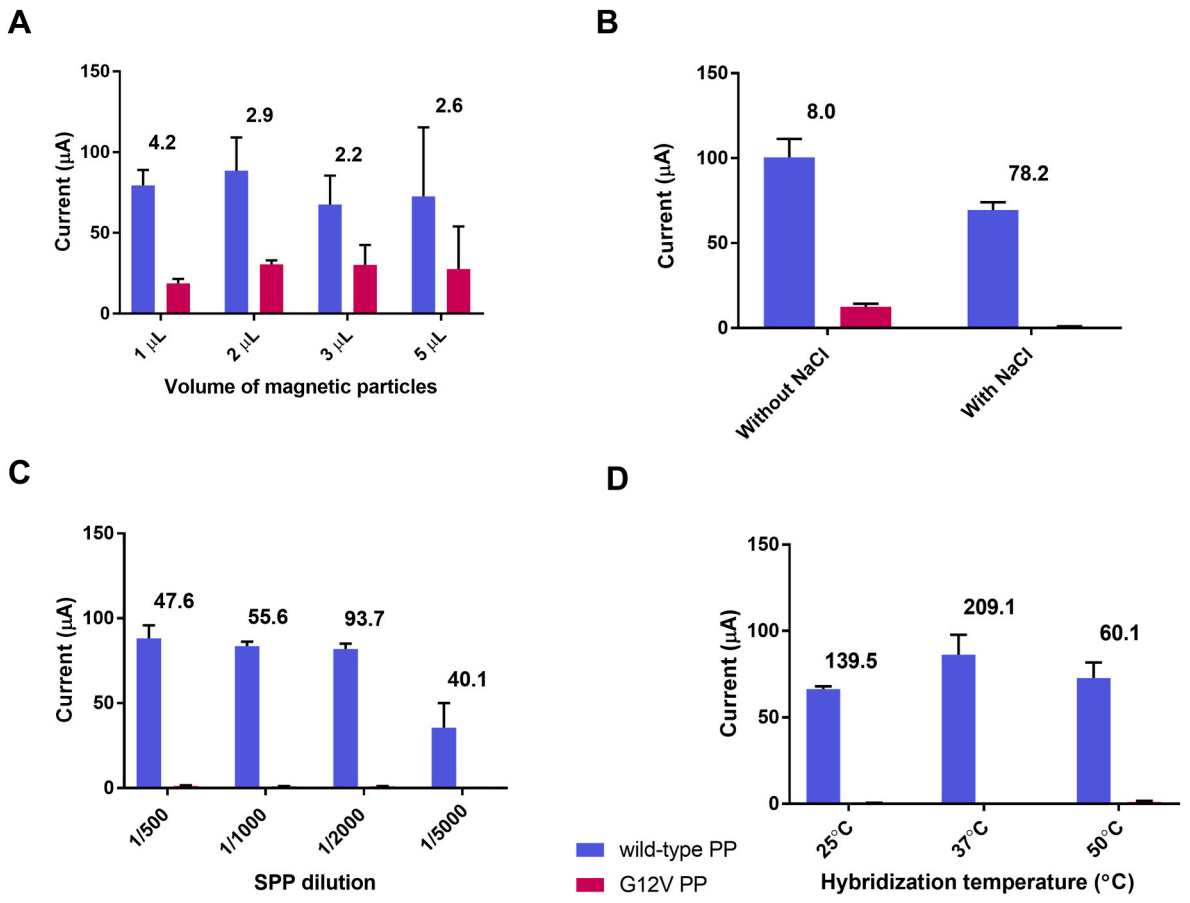

Fig. 2. Optimization studies with 100 nM synthetic wt target duplex using two different padlock probes, i.e., wt PP (blue bars) and G12V PP (red bars). (A) Optimization of magnetic particles volume per sample. (B) Comparison of EC signals with and without 0.2 M NaCl during ligation reaction. (C) Optimization of SPP dilution (diluted in casein blocking buffer). (D) Comparison of different temperatures during hybridization between RCA products and LNA-modified MPs. All studies were performed in duplicates. Values above error bars denote signal-to-noise ratios (ratios of EC signals between wt PP and G12V PP samples).

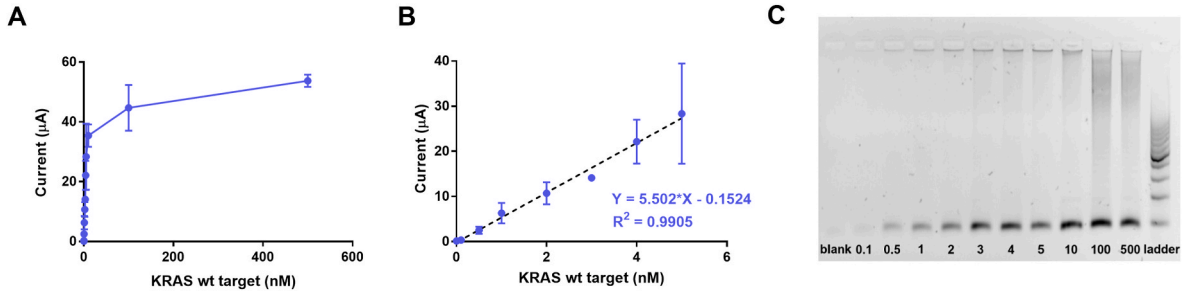

Fig. 3. Analytical sensitivity of the bioassay (B_{wt}). (A) Dependence of electric current values on concentration of wt target duplex (using wt PP and wtLNA CPs). (B) Linear region of the concentration dependence with regression analysis showing the linear equation and coefficient of determination (R^2). (C) An image agarose gel showing different concentrations of RCA products, corresponding to the values in (A). A 100 bp ladder was used.

yielding a relative standard deviation (RSD) of 13.38 %. We found a strong correlation between the EC bioassay and gel electrophoresis results (Fig. 3C); however, gel electrophoresis showed lower sensitivity, with bands undetectable below 2 nM, while the EC assay achieved a superior LOD of 61 pM (Fig. 3B).

The selectivity of the EC assay was assessed to determine its capacity to differentiate between target DNA (wt *KRAS*) and non-specific sequences. A series of negative control experiments were conducted using *KRAS* B_{wt} to analyze DNA sequences from different genes, including wt *BRAF*, V600E *BRAF*, HPV16 and HPV18 sequences. Moreover, *KRAS* G12V sequence as well as a non-template (blank) sample was added alongside the positive control target DNA to evaluate the assay's response to potential non-specific binding (Fig. 4A). Measurements were performed in duplicates. The results confirmed the assay's excellent selectivity. A strong amperometric signal was observed for the target DNA, while signals for mismatched or non-complementary sequences were negligible (see amperograms in Fig. 4A inset). The same panel of DNA sequences was applied also to *KRAS* B_{G12V}, and as expected, the only positive signal was obtained only for G12V target, while all other sequences gave negligible signals (Fig. 4A). The signals were markedly lower not only for non-complementary sequences, but also for single-base mismatches, underscoring the assay's high specificity in detecting the exact target sequence. This selectivity is attributed to the use of highly specific recognition elements, such as LNA-modified probes and

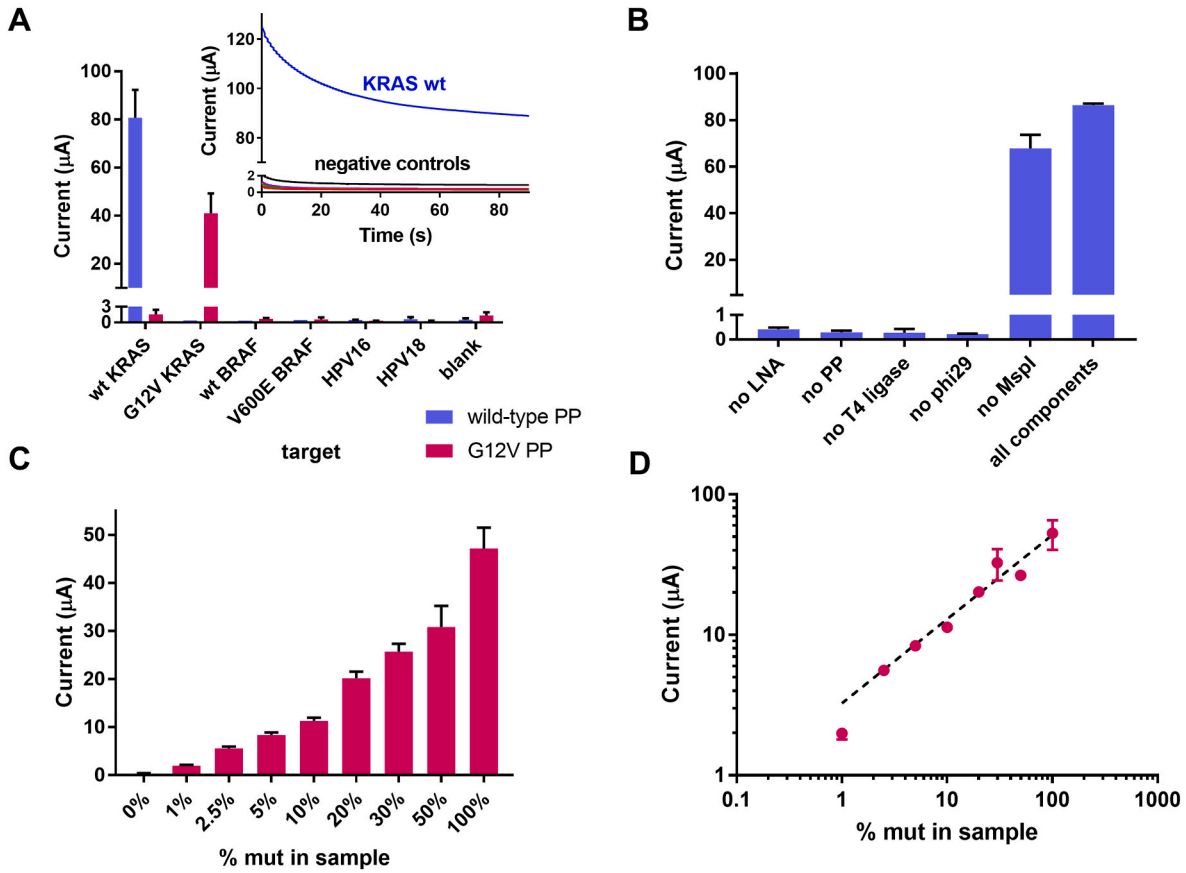

Fig. 4. Analytical characteristics of the bioassay. (A) Selectivity of wt PP (blue bars) and G12V PP (red bars) towards various synthetic targets, including positive controls (wt target for wt *KRAS*; G12V *KRAS* for G12V PP), the rest being negative controls (mismatched *KRAS* target, wt *BRAF* and V600E mutated *BRAF* target, HPV16 and HPV18 and blank as a non-template control). Inset: Raw amperograms for wt PP-containing samples. (B) A component removal experiment demonstrating importance of all reagents for successful analysis (except MspI enzyme, which is not required but recommended). The sample was a wt *KRAS* with wt PP. (C) The spiking experiment showing incremental addition of G12V target (mut) into an excess of wt target (100 nM). 0 % sample means no added G12V target, 1 % sample means a mixture of 1 nM G12V and 100 nM wt target, etc. (D) A goodness-of-fit model using log-log linear regression for same samples as in (C).

optimized hybridization conditions, which together enhance the assay's ability to distinguish closely related sequences.

To further evaluate the assay performance, a component removal experiment was carried out to analyze the impact of each individual component. This involved systematically omitting one component at a time, such as LNA (i.e., only unmodified MPs were added to the reaction), PP, T4 ligase, phi29 polymerase, and MspI enzyme, while keeping all other assay conditions constant. A full assay with all components served as the control. The results demonstrated that most components were essential to assay fabrication, as the signal was significantly reduced or absent when the component was removed (Fig. 4B). The only exception was the MspI enzyme; even without this endonuclease, some level of discrimination remained, since the undigested RCA product could still bind to the LNA probe. However, omitting MspI led to visible aggregation of the MP-LNA CPs, likely due to interactions between the MP-LNA and the RCA amplicons' long concatenated structures [31]. This aggregation impacted assay reproducibility and resulted in some signal loss. Therefore, despite adding 30 min to the assay, the MspI digestion step was retained to ensure assay stability and reliability.

The tumor tissue sample from a patient is usually highly heterogeneous and the mutation is not always present in all the cells within the biopsy [32]. For instance, adjacent healthy tissue without a mutation is collected alongside the tumor, which makes the determination challenging [33,34]. To quantitatively evaluate the capacity of our strategy to correctly identify trace amounts of mutated sequence in an excess of a wt sample, the G12V template DNA was incrementally spiked into the wt target at ratios of 0 %, 1 %, 2.5 %, 5 %, 10 %, 20 %, 30 %, 50 %, and 100 %, and the amperometric signals were recorded (plotted as bar graphs in Fig. 4C). The calibration plot in Fig. 4D showed strong linearity when plotted as log-log line ($R^2 = 0.89$) that allowed determination of as little as 1 % of G12V mutation in the sample. The limit of detection calculated as 3 × SD of blank measurements (i.e., 0 % of mut sample) was 0.53 % of G12V DNA in high excess of wt DNA, demonstrating the assay's strong discrimination capability.

3.4. Real sample analysis

Ultimately, we have applied our optimized assay to analyze *KRAS* mutation in 7 cancer cell lines and 11 colorectal cancer patients' samples, all with known mutation status (Fig. 5A). Regarding cell lines, those with wt sequence (HT-29, A-375, CaSki and HeLa) yielded high EC signals only when using wt PP, while two cell lines with G12V mutation (SW480 and SW620) yielded visible EC signals only for G12V PP. Two additional cell lines bearing other *KRAS* mutations (A549 with G12S, DLD-1 with G13D) gave low EC signals for both padlocks. In case of clinical samples, we gathered a small patient cohort having either wt (5 samples) or G12V (6 samples) sequences (identified with NGS). Similarly, as for the cell lines, the EC signals perfectly agreed with the NGS data, i.e., those samples with G12V mutation yielded visible EC signals only for G12V padlock, and vice versa for wt sequence. Fig. 5 shows also EC signals for synthetic targets using both padlocks, serving as positive (matching target and PP) and negative controls (nonmatching targets and PPs), as well as non-template control. As expected, EC signals for synthetic targets were much higher than for real samples, due to variable

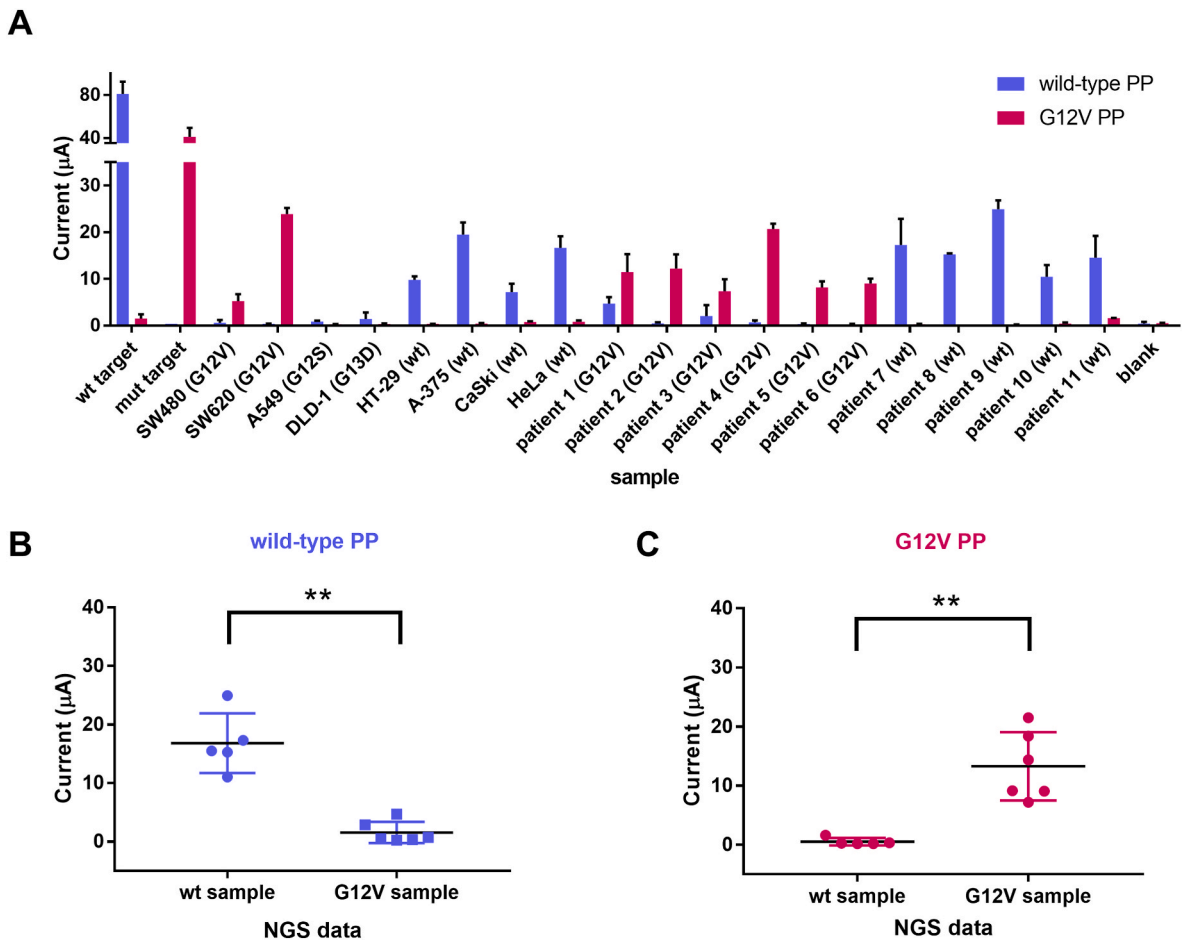

Fig. 5. Real samples analysis comprising 8 cell lines and 11 CRC patient samples with known *KRAS* status. Two synthetic positive controls (wt target and G12V mut target) and blank (non-template control) were also used. (A) Bar graph showing means of duplicate measurements for both wt PP (blue) and G12V PP (red). (B–C) Dot plot graphs comparing EC values for (B) wt PP and (C) G12V PP. The samples were divided into two groups (wt and G12V) based on NGS data. Each dot represents the mean value from duplicate EC measurements. The difference between these two groups was significant ($p < 0.005$, flagged with two stars).

quality and lower amounts of DNA obtained from cell lines and patients. Nevertheless, an RPA-preamplification step followed by RCA was sufficient for final analysis.

Fig. 5 also shows dot plots with either wt PP (Fig. 5B) or G12V PP (Fig. 5C). In these plots, clinical samples were divided into two groups based on NGS data (wt group on the left, and G12V group on the right). Each dot represents the mean value from duplicate EC measurements. Our EC assay correctly identified all wt and G12V samples for both padlocks; moreover, the differences between wt and G12V samples obtained with our method were statistically significant, reaching p-values <0.005.

Previous studies have reported EC-based detection of *KRAS* mutation, involving PCR [35], RCA, hybridization chain reaction [36] or without any amplification [37]. Despite reaching lower limits of detection than our assay, none of them have applied the assays into real patient samples, but instead used only spiking of synthetic DNA into human serum. An excellent study was performed by Das et al. who used a PNA clamping strategy to develop a rapid electrochemical assay that discriminates mutations in human serum, targeting seven most frequent mutations in the *KRAS* gene and V600E mutation in the *BRAF* gene [38].

Table 2
Comparison of our work with other EC assays for *KRAS* detection.

KRAS mutation	Strategy	Limit of detection	Sample type	Dual detection	Ref.
G12D	PCR coupled with T7 endonuclease-mediated voltammetry	11.89 fM	Cell lines	No	[35]
not specified	exonuclease III-assisted target recycling and RCA	0.28 fM	Synthetic DNA spiked in human serum	No	[36]
G12D	anchor-like DNA EC biosensor	0.1 pM	Synthetic DNA spiked in human serum	No	[37]
multiple KRAS mutations	peptide nucleic acid clamp assay chip	1 fg μl^{-1}	Cell-free nucleic acid (cfDNA and cfRNA) in serum samples from lung cancer patients	No	[38]
G12D	Nanocomposites-based toehold-mediated DNA strand displacement	0.38 fM	Synthetic DNA spiked in human serum	No	[39]
not specified	carboxylated multi-walled carbon nanotube/ molybdenum disulfide composites	3 fM	Synthetic DNA spiked in human serum	No	[40]
G12C	label-free impedance biosensor	86.9 fM	Synthetic DNA spiked in human serum	No	[41]
G12V	Amperometry coupled with RCA and LNA probes	61 pM	Tissue samples from CRC and melanoma patients	Yes	This work

This was one of few reports that involved real patient samples, although they targeted lung cancer and melanoma, but not CRC. Table 2 provides a comparative analysis of our study and other EC-based assays for *KRAS* mutation detection. While our limit of detection is not as low as that achieved by some other methods, our bioassay is among the few that utilize real patient samples. Moreover, it is the only approach that enables parallel analysis of both wt and mutated sequences, thereby minimizing the risk of false negatives.

3.5. Logistic regression classification results

We trained and evaluated classifiers in two settings: in the first setting, we used only clinical samples which are either wt or have the G12V mutation, so that the model is trained to discriminate between samples exhibiting the G12V mutation and no mutation. In the second setting, we used both the samples and cell lines, including the two cell lines with other mutations, and the classifier was trained to classify G12V as target while, other mutations - along with no mutation - were considered non-target.

Fig. 6A and B shows the plot of the logistic regression classifier's receiver operating characteristics (ROC) for the pair of experiments. The ROC plots were obtained by aggregating the classifier predictions (i.e., probability values between 0 and 1 that the mutation was detected) across cross-validation folds and comparing them to the ground truth (whether or not the mutation actually occurred). In both settings, we observed perfect classification accuracy, which supports the fact that the logarithms of the signals from the wt and mutated samples were linearly separable. We also noticed that for the second experiment, where cell lines with other, non-G12V mutations were included, using the logarithms of the current readouts as input features was useful for obtaining perfect performance; in an alternative system where we used the current values directly, we observed perfect detection performance for the first experiment but imperfect, albeit very high detection rates, for the second experiment with an ROC having an area of 0.998 (not shown).

We further analyzed the features learned by the classifier and plotted the weights learned for each timestep in Fig. 6C and D. The lines show the average (across cross-validation folds) learned weight for each timestep and padlock. We observed that the model, in general, learns to assign positive weights to readings from the G12V PP. In the setting with only clinical samples where no non-G12V mutations are present (Fig. 6C), the model tends to assign weights symmetrically between the two padlocks with negative weighting of the wt PP signal, across the length of the measurements, i.e. the model learns to classify samples with high readout on the wt PP as nontarget. In the other setting, where non-G12V mutations were included (Fig. 6D), the model assigns values relatively close to zero to the wt signal. This is a consequence of having to also classify samples with other mutations as nontarget despite their low current readout on the wt PP.

4. Conclusion

In this study, we have successfully combined RCA reaction with amperometric readout to simultaneously analyze either wt sequence or G12V mutation in *KRAS* gene in a rapid and simple manner. The bioassay displayed good analytical sensitivity and excellent selectivity towards G12V mutation, enabling us to detect <1 % of G12V sequence

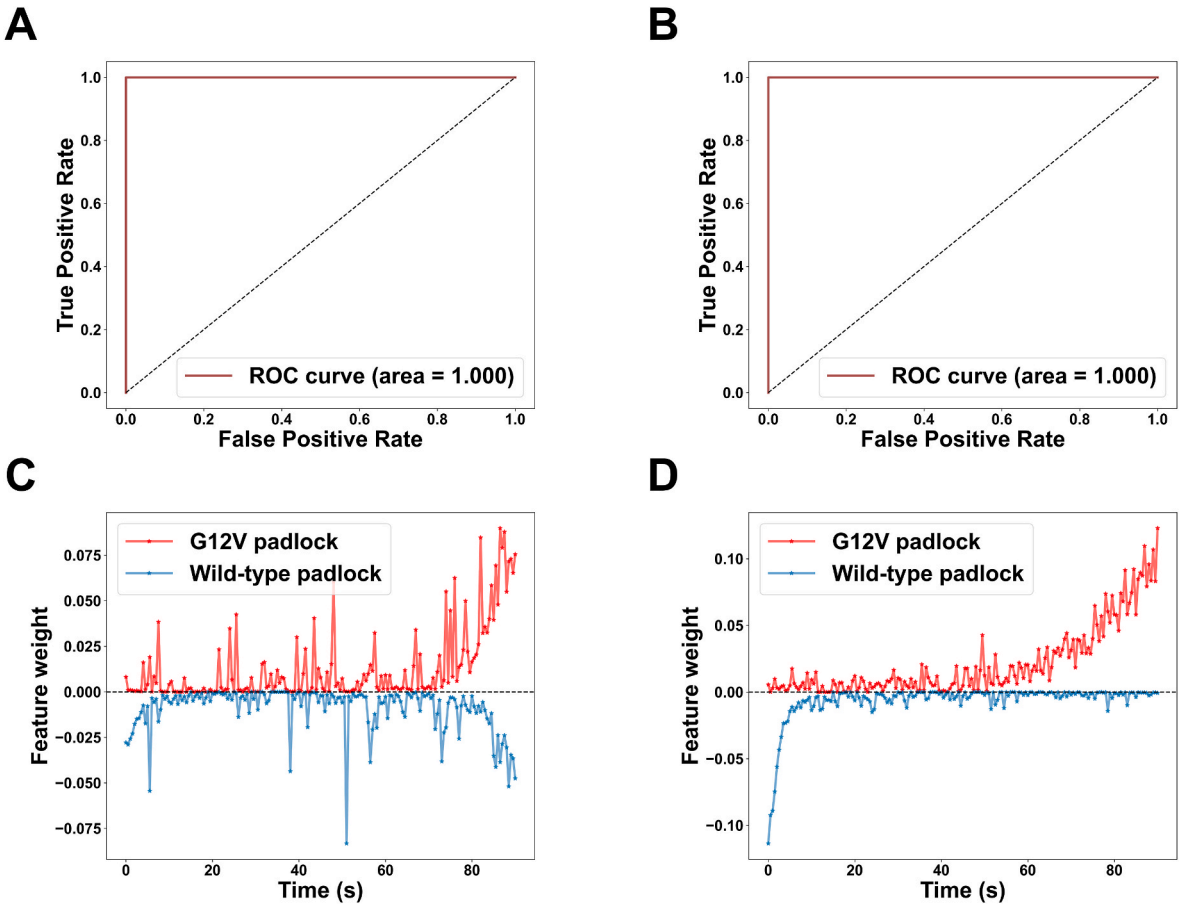

Fig. 6. Results of the logistic regression classifier aggregated over cross-validation runs. (A–B) ROC curves for classifiers trained and evaluated on (A) only clinical samples and (B) clinical samples and cell lines. (C–D) Average learned weights for (C) clinical samples and (D) clinical samples and cell lines with weights of the G12V PP in red and weights of the wt PP in blue.

in the excess of wt sample. This is a critical step towards future liquid biopsy analysis of circulating tumor DNA, which is often found in very low levels compared to wt circulating free DNA (often in a range 0.5 %–10 % depending on the stage of the tumor) [42]. Although other EC-based studies showed lower limits of detection (described in previous section), majority of them lacked validation using patient samples and strict comparison with standard techniques. In our study, we showed very good performance using 11 patient samples and 7 cancer cell lines with known mutation status, clearly discriminating wt from G12V sequences. To make the bioassay even more straightforward, we automated a decision-making process by utilizing logistic regression analysis. As opposed to other, more complex machine learning models such as support vector machines or deep neural networks used in recent biosensors studies [43–47], this approach is simpler because the signals from our assays are already separable without any nonlinear transformations. Moreover, the simplicity of logistic regression has the added advantage that its decision-making can be easily analyzed by directly inspecting its weights, making it transparent and interpretable to human oversight. To counter the difficulty of making statistical inferences in this data-scarce setting, we used leave-pair-out cross-validation to analyze the performance of the proposed classifier, showing that a linear model is enough to classify the signals from the bioassay.

This study should be considered only as a proof-of-concept and we are aware that by including more patient samples, the statistical analysis would be more powerful. Hence, this is only a first step towards more complex *KRAS* gene analysis; in following study, we wish to expand the G12V mutation to other clinically relevant *KRAS* mutations, such as G12C [48] or G13D [49], include more patient samples, and exploit an option to combine all pre-amplification steps into one tube (by mixing PPs) to minimize sample consumption and simplify overall protocol. In conclusion, the combination of isothermal techniques, simple inexpensive electrochemical instrumentation and AI-assisted tool makes the assay potentially useful in more decentralized or low-resource settings by avoiding thermal cycling and bulky equipment.

CRediT authorship contribution statement

Ravery Sebuyoya: Writing – review & editing, Writing – original draft, Visualization, Validation, Methodology, Investigation, Conceptualization. **Sarka Sevcikova:** Writing – review & editing, Validation, Investigation. **Bolaji Yusuf:** Writing – review & editing, Visualization, Methodology, Investigation. **Martin Bartosik:** Writing – review & editing, Writing – original draft, Visualization, Supervision, Methodology, Funding acquisition, Conceptualization.

Declaration of competing interest

The authors declare that they have no known competing financial interests or personal relationships that could have appeared to influence the work reported in this paper.

Acknowledgements

The financial support of the Czech Health Research Council (No. NU21-08-00078), Czech Science Foundation (No. 25-15990S), project SALVAGE (OP JAC; reg. no. CZ.02.01.01/00/22_008/0004644) – co-funded by the European Union and by the State Budget of the Czech Republic, BBMRI.cz (No. LM2023033) and MH CZ – DRO (MMCI, 00209805) is greatly acknowledged. Bolaji Yusuf was partly supported by Brno University of Technology internal project No. FIT-S-23-8278.

Data availability

Data will be made available on request.

References

[1] X. Liu, M. Jakubowski, J.L. Hunt, KRAS gene mutation in colorectal cancer is correlated with increased proliferation and spontaneous apoptosis, Am. J. Clin. Pathol. 135 (2) (2011) 245–252, https://doi.org/10.1309/AJCP7FO2VAXIVSTP.
[2] D. Modest, I. Ricard, V. Heinemann, S. Hegewisch-Becker, W. Schmiegel, R. Porschen, S. Stintzing, U. Graeven, D. Arnold, L. Fischer von Weikersthal, C. Giessen-Jung, A. Stahler, H.-J. Schmoll, A. Jung, T. Kirchner, A. Tannapfel, A. Reinacher-Schick, Outcome according to KRAS-, NRAS- and BRAF-mutation as well as KRAS mutation variants: pooled analysis of five randomized trials in metastatic colorectal cancer by the AIO colorectal cancer study group, Ann. Oncol. 27 (2016) 261, https://doi.org/10.1093/annonc/mdw261.
[3] W. De Roock, V. Vriendt, N. Normanno, F. Ciardiello, S. Tejpar, KRAS, BRAF, PIK3CA, and PTEN mutations: implications for targeted therapies in metastatic colorectal cancer, Lancet Oncol. 12 (2010) 594–603, https://doi.org/10.1016/S1470-2045(10)70209-6.
[4] M. Meng, K. Zhong, T. Jiang, Z. Liu, H.Y. Kwan, T. Su, The current understanding on the impact of KRAS on colorectal cancer, Biomed. Pharmacother. 140 (2021) 111717, https://doi.org/10.1016/j.biopha.2021.111717.
[5] Q. Ai, F. Li, S. Zou, Z. Zhang, Y. Jin, L. Jiang, H. Chen, X. Deng, C. Peng, N. Mou, C. Wen, B. Shen, Q. Zhan, Targeting KRASG12V mutations with HLA class II-restricted TCR for the immunotherapy in solid tumors, Front. Immunol. 14 (2023), https://doi.org/10.3389/fimmu.2023.1161538.
[6] Andrew G. Stephen, D. Esposito, Rachel K. Bagni, F. McCormick, Dragging ras back in the ring, Cancer Cell 25 (3) (2014) 272–281, https://doi.org/10.1016/j.ccr.2014.02.017.
[7] R. Veluswamy, P.C. Mack, J. Houldsworth, E. Elkhouly, F.R. Hirsch, KRAS G12C–mutant non–small cell lung cancer: biology, developmental therapeutics, and molecular testing, J. Mol. Diagn. 23 (5) (2021) 507–520, https://doi.org/10.1016/j.jmoldx.2021.02.002.
[8] D. Lu, Y. Chen, M. Jiang, J. Wang, Y. Li, K. Ma, W. Sun, X. Zheng, J. Qi, W. Jin, Y. Chen, Y. Chai, C.W.H. Zhang, H. Liang, S. Tan, G.F. Gao, KRAS G12V neoantigen specific T cell receptor for adoptive T cell therapy against tumors, Nat. Commun. 14 (1) (2023) 6389, https://doi.org/10.1038/s41467-023-42010-1.
[9] J. Luo, J. Ostrem, B. Pellini, D. Imbody, Y. Stern, H.S. Solanki, E.B. Haura, L. C. Villaruz, Overcoming KRAS-mutant lung cancer, Am Soc Clin Oncol Educ Book (42) (2022) 700–710, https://doi.org/10.1200/EDBK_360354.
[10] H.-S. Kou, K.-H. Lin, R. Sebuyoya, K.-S. Chueh, C.-W. Cheng, C.-C. Wang, Dual-probe ligation without PCR for fluorescent sandwich assay of EGFR nucleotide variants in magnetic gene capture platform, Microchim. Acta 190 (9) (2023) 375, https://doi.org/10.1007/s00604-023-05950-5.
[11] S. Wang, S. Lu, J. Zhao, J. Ye, J. Huang, X. Yang, An electric potential modulated cascade of catalyzed hairpin assembly and rolling chain amplification for microRNA detection, Biosens. Bioelectron. 126 (2019) 565–571, https://doi.org/10.1016/j.bios.2018.09.088.
[12] M. Ortiz, M. Jauset-Rubio, D. Kodr, A. Simonova, M. Hocek, C.K. O'Sullivan, Solid-phase recombinase polymerase amplification using ferrocene-labelled dNTPs for electrochemical detection of single nucleotide polymorphisms, Biosens. Bioelectron. 198 (2022) 113825, https://doi.org/10.1016/j.bios.2021.113825.
[13] T. Wang, Q. Peng, B. Guo, D. Zhang, M. Zhao, H. Que, H. Wu, Y. Yan, An integrated electrochemical biosensor based on target-triggered strand displacement amplification and "four-way" DNA junction towards ultrasensitive detection of PIK3CA gene mutation, Biosens. Bioelectron. 150 (2020) 111954, https://doi.org/10.1016/j.bios.2019.111954.
[14] C. Wang, J. Yu, L. Qi, J. Yu, M. Yang, Y. Du, Glucometer-based ultra-sensitive BRAF V600E mutation detection facilitated by magnetic nanochains and a self-made point-of-care (POC) device, Electroanalysis 34 (2) (2022) 294–301, https://doi.org/10.1002/elan.202100286.
[15] Y. Zhao, F. Chen, Q. Li, L. Wang, C. Fan, Isothermal amplification of nucleic acids, Chem. Rev. 115 (22) (2015) 12491–12545, https://doi.org/10.1021/acs.chemrev.5b00428.
[16] M. Ali, F. Li, Z. Zhang, K. Zhang, D.-K. Kang, J. Ankrum, X.C. Le, W. Zhao, Rolling circle amplification: a versatile tool for chemical biology, materials science and medicine, Chem. Soc. Rev. 43 (2014), https://doi.org/10.1039/C3CS60439J.
[17] S. Lee, J. You, I. Baek, H. Park, K. Jang, C. Park, S. Na, Synergistic enhanced rolling circle amplification based on mutS and radical polymerization for single-point mutation DNA detection, Biosens. Bioelectron. 210 (2022) 114295, https://doi.org/10.1016/j.bios.2022.114295.
[18] Q. Wang, C. Yang, Y. Xiang, R. Yuan, Y. Chai, Dual amplified and ultrasensitive electrochemical detection of mutant DNA Biomarkers based on nuclease-assisted target recycling and rolling circle amplifications, Biosens. Bioelectron. 55 (2014) 266–271, https://doi.org/10.1016/j.bios.2013.12.034.
[19] K. Ondraskova, R. Sebuyoya, L. Moranova, J. Holcakova, P. Vonka, R. Hrstka, M. Bartosik, Electrochemical biosensors for analysis of DNA point mutations in cancer research, Anal. Bioanal. Chem. 415 (6) (2023) 1065–1085, https://doi.org/10.1007/s00216-022-04388-7.
[20] D. Li, Y. Xu, L. Fan, B. Shen, X. Ding, R. Yuan, X. Li, W. Chen, Target-driven rolling walker based electrochemical biosensor for ultrasensitive detection of circulating tumor DNA using doxorubicin@tetrahedron-Au tags, Biosens. Bioelectron. 148 (2020) 111826, https://doi.org/10.1016/j.bios.2019.111826.
[21] Y. Geng, J. Wu, L. Shao, F. Yan, H. Ju, Sensitive colorimetric biosensing for methylation analysis of p16/CDKN2 promoter with hyperbranched rolling circle amplification, Biosens. Bioelectron. 61 (2014) 593–597, https://doi.org/10.1016/j.bios.2014.06.010.
[22] R. Sebuyoya, A. Valverde, L. Moranova, J. Strmiskova, R. Hrstka, V.R.-V. Montiel, J.M. Pingarrón, R. Barderas, S. Campuzano, M. Bartosik, Dual detection system for

cancer-associated point mutations assisted by a multiplexed LNA-based amperometric bioplatform coupled with rolling circle amplification, Sensor. Actuator. B Chem. 394 (2023) 134375, https://doi.org/10.1016/j.snb.2023.134375.

[23] F. Pedregosa, G. Varoquaux, A. Gramfort, V. Michel, B. Thirion, O. Grisel, M. Blondel, P. Prettenhofer, R. Weiss, V. Dubourg, J. Vanderplas, A. Passos, D. Cournapeau, M. Brucher, M. Perrot, E. Duchesnay, G. Louppe, Scikit-learn: machine learning in Python, J. Mach. Learn. Res. 12 (2012), https://doi.org/10.48550/arXiv.1201.0490.

[24] P. Gaspers, P. Lemke, A. Delavault, C.M. Domínguez, K. Rabe, C. Niemeyer, Engineering phi29-DNAP variants for customized DNA hydrogel materials, Chem. Eur J. (2024) e202403047, https://doi.org/10.1002/chem.202403047.

[25] Y. Yoshino, M. Ishida, A. Horii, A new 10-min ligation method using a modified buffer system with a very low amount of T4 DNA ligase: the "Coffee Break Ligation" technique, Biotechnol. Lett. 29 (10) (2007) 1557–1560, https://doi.org/10.1007/s10529-007-9429-z.

[26] M. Anton, L. Moráňová, M. Bartošík, Application of electrochemical LAMP-based assay for screening of HPV16/HPV18 infection in cervical samples, Anal. Methods 12 (2020), https://doi.org/10.1039/C9AY02383F.

[27] M. Bartosik, L. Jirakova, M. Anton, B. Vojtesek, R. Hrstka, Genomagnetic LAMP-based electrochemical test for determination of high-risk HPV16 and HPV18 in clinical samples, Anal. Chim. Acta 1042 (2018) 37–43, https://doi.org/10.1016/j.aca.2018.08.020.

[28] N. Izadi, R. Sebuyoya, L. Moranova, R. Hrstka, M. Anton, M. Bartosik, Electrochemical bioassay coupled to LAMP reaction for determination of high-risk HPV infection in crude lysates, Anal. Chim. Acta 1187 (2021) 339145, https://doi.org/10.1016/j.aca.2021.339145.

[29] N. Izadi, J. Strmiskova, M. Anton, J. Hausnerova, M. Bartosik, LAMP-based electrochemical platform for monitoring HPV genome integration at the mRNA level associated with higher risk of cervical cancer progression, J. Med. Virol. 96 (10) (2024) e70008, https://doi.org/10.1002/jmv.70008.

[30] L. Moráňová, J. Strmiskova, K. Ondrášková, M. Bardelčík, M. Cwik, I. Kiss, M. Bartosik, Electrochemical detection of BRAF V600E mutation in a liquid biopsy format: LAMPing the way to an improved diagnostics and treatment, Adv Mater Technol (2024), https://doi.org/10.1002/admt.202401404.

[31] D. Sánchez Martín, R. Oropesa-Nuñez, T. Zardán Gómez de la Torre, Formation of visible aggregates between rolling circle amplification products and magnetic nanoparticles as a strategy for point-of-care diagnostics, ACS Omega 6 (48) (2021) 32970–32976, https://doi.org/10.1021/acsomega.1c05047.

[32] X. Sagaert, A. Vanstapel, S. Verbeek, Tumor heterogeneity in colorectal cancer: what do we know so far? Pathobiology 85 (1–2) (2018) 72–84, https://doi.org/10.1159/000486721.

[33] C. Fiala, E.P. Diamandis, Mutations in normal tissues—some diagnostic and clinical implications, BMC Med. 18 (1) (2020) 283, https://doi.org/10.1186/s12916-020-01763-y.

[34] B. Weber, P. Meldgaard, H. Hager, L. Wu, W. Wei, J. Tsai, A. Khalil, E. Nexo, B. S. Sorensen, Detection of EGFR mutations in plasma and biopsies from non-small cell lung cancer patients by allele-specific PCR assays, BMC Cancer 14 (1) (2014) 294, https://doi.org/10.1186/1471-2407-14-294.

[35] P. Chowdhury, B.S. Cha, S. Kim, E.S. Lee, T. Yoon, J. Woo, K.S. Park, T7 Endonuclease I-mediated voltammetric detection of KRAS mutation coupled with horseradish peroxidase for signal amplification, Microchim. Acta 189 (2) (2022) 75, https://doi.org/10.1007/s00604-021-05089-1.

[36] Q. Xiao, J. Feng, J. Li, Y. Liu, D. Wang, S. Huang, Ratiometric electrochemical biosensor for ultrasensitive and highly selective detection of K-ras gene via exonuclease III-assisted target recycling and rolling circle amplification strategies, Anal. Methods 11 (2019), https://doi.org/10.1039/C9AY01007F.

[37] N. Zeng, J. Xiang, Detection of KRAS G12D point mutation level by anchor-like DNA electrochemical biosensor, Talanta 198 (2019) 111–117, https://doi.org/10.1016/j.talanta.2019.01.105.

[38] J. Das, I. Ivanov, L. Montermini, J. Rak, E. Sargent, S. Kelley, An electrochemical clamp assay for direct, rapid analysis of circulating nucleic acids in serum, Nat. Chem. 7 (2015), https://doi.org/10.1038/nchem.2270.

[39] X. Yu, S. Bai, L. Wang, In situ reduction of gold nanoparticles-decorated MXenes-based electrochemical sensing platform for KRAS gene detection, Front. Bioeng. Biotechnol. 11 (2023), https://doi.org/10.3389/fbioe.2023.1176046.

[40] X. Wang, M. Yang, Q. Liu, S. Yang, X. Geng, Y. Yang, H. Fa, Y. Wang, C. Hou, An ultrasensitive electrochemical DNA biosensor based on carboxylated multi-walled carbon nanotube/molybdenum disulfide composites for KRAS gene detection, Anal. Sci. 35 (4) (2019) 441–448, https://doi.org/10.2116/analsci.18P518.

[41] Y. Zhang, H. Wei, L. Guo, W. Gao, D. Cheng, Y. Liu, A novel label-free impedance biosensor for KRAS G12C mutations detection based on PET-RAFT and ROP synergistic signal amplification, Bioelectrochemistry 161 (2025) 108844, https://doi.org/10.1016/j.bioelechem.2024.108844.

[42] V. Taly, D. Pekin, L. Benhaim, S.K. Kotsopoulos, D. Le Corre, X. Li, I. Atochin, D. R. Link, A.D. Griffiths, K. Pallier, H. Blons, O. Bouché, B. Landi, J.B. Hutchison, P. Laurent-Puig, Multiplex picodroplet digital PCR to detect KRAS mutations in circulating DNA from the plasma of colorectal cancer patients, Clin. Chem. 59 (12) (2013) 1722–1731, https://doi.org/10.1373/clinchem.2013.206359.

[43] J. Massah, K. Asefpour Vakilian, An intelligent portable biosensor for fast and accurate nitrate determination using cyclic voltammetry, Biosyst. Eng. 177 (2019) 49–58, https://doi.org/10.1016/j.biosystemseng.2018.09.007.

[44] T. Hui, D. Xiang, S.H.-S. Loh, T. Maul, M. Tan, Graphene/TiO 2 nanocomposite based electrochemical biosensor enhanced by support vector machine classification model to detect different DENV serotype IgG, 1-4, https://doi.org/10.1109/SENSORS56945.2023.10325156, 2023.

[45] P. Moitra, A. Chaichi, S.M. Abid Hasan, K. Dighe, M. Alafeef, A. Prasad, M. R. Gartia, D. Pan, Probing the mutation independent interaction of DNA probes with SARS-CoV-2 variants through a combination of surface-enhanced Raman scattering and machine learning, Biosens. Bioelectron. 208 (2022) 114200, https://doi.org/10.1016/j.bios.2022.114200.

[46] O. Guselnikova, A. Trelin, A. Skvortsova, P. Ulbrich, P. Postnikov, A. Pershina, D. Sykora, V. Svorcik, O. Lyutakov, Label-free surface-enhanced Raman spectroscopy with artificial neural network technique for recognition photoinduced DNA damage, Biosens. Bioelectron. 145 (2019) 111718, https://doi.org/10.1016/j.bios.2019.111718.

[47] Z. Guo, R. Tian, W. Xu, D. Yip, M. Radyk, F.B. Santos, A. Yip, T. Chen, X.S. Tang, Highly accurate heart failure classification using carbon nanotube thin film biosensors and machine learning assisted data analysis, Biosens. Bioelectron. X 12 (2022) 100187, https://doi.org/10.1016/j.biosx.2022.100187.

[48] T.-R. Peng, T.-W. Wu, T.-Y. Yi, A.-J. Wu, Comparative efficacy of adagrasib and sotorasib in KRAS G12C-mutant NSCLC: insights from pivotal trials, Cancers 16 (2024) 3676, https://doi.org/10.3390/cancers16213676.

[49] S. Kumar, T. Price, O. Mohyieldin, M. Borg, A. Townsend, J. Hardingham, KRAS G13D mutation and sensitivity to cetuximab or panitumumab in a colorectal cancer cell line model, Gastroint Cancer Res 7 (2014) 23–26.